J. Fluid Mech. (2007), *vol.* 578, *pp.* 95–112.
doi:10.1017/S0022112007004661 Printed in the United Kingdom

Bi-directional flows in constrained systems

HERBERT E. HUPPERT AND MARK A. HALLWORTH

Institute of Theoretical Geophysics, Department of Applied Mathematics and Theoretical Physics, University of Cambridge, Centre for Mathematical Sciences, Wilberforce Road, Cambridge CB3 0WA, UK

heh1@esc.cam.ac.uk; hallwort@esc.cam.ac.uk

(Received 23 December 2005 and in revised form 16 November 2006)

We consider the exchange flow of relatively dense, viscous fluid in a container connected by a vertical pipe to a container beneath it, initially full of relatively light fluid. A non-dimensional value for the flux of dense fluid down the tube is determined experimentally as a function of the ratio of the two viscosities and the Reynolds number. The experimental data are satisfactorily collapsed using dimensional analysis and balancing buoyancy, inertial and viscous forces as appropriate. A theoretical analysis, assuming steady, axisymmetric motion, captures a considerable part, but not all of the processes involved. The paper discusses quantitative applications of the results to the movement of magma in volcanic conduits. The concepts indicate how bi-directional convection in the conduit between a lava lake and a magma reservoir deep in the crust is the essential ingredient in the explanation of the long-standing problem that the amount of degassing of sulphur dioxide from a lava lake in a volcanic crater can exceed by many orders of magnitude that consistent with the amount of lava solidified in the crater. Movies are available with the online version of the paper.

1. Introduction

Uni-directional, steady flow along a horizontal pipe of constant cross-section (neglecting the effects of gravity) is one of the fundamental problems in fluid mechanics (Batchelor 1967). Under these circumstances, with applied pressures at either end, it is impossible to have a bi-directional flow. However, for a flow in a diverging channel, known as Jeffrey–Hammel flow, beyond a certain flux dependent on the Reynolds number, the flow can become so concentrated at the axis that there is a return flow close to the walls (Batchelor 1967).

The flow of two different fluids along a pipe has been extensively investigated, by (amongst others) Hickox (1971), Scoffoni, Lajeunesse & Homsy (2001) and D. D. Joseph and his co-workers (see, for example, Joseph *et al.* 1997), motivated in part by the interest of oil companies in pumping viscous oils through pipelines. The inclusion of water, whose viscosity is very much less than the oil, can considerably reduce the pressure needed to pump a given flux of oil through the pipe by lubricating the high shear region near the wall. The flow in such situations is rarely, if ever, stable and breaks up into a series of different flow types, which are reviewed by Joseph *et al.* (1997) and include the formation of bubbles, slugs, bamboo waves and what Joseph calls disturbed core-annular flow. These studies have concentrated on the flow patterns generated by counterflows in a tube, while we focus here on the initial exchange rate between the two reservoirs linked by the tube, rather than the flow details.

In a related problem, Stevenson & Blake (1998) presented experimental results for the evolution in a long thin tube of a lower region of viscous fluid initially overlain by viscous fluid of greater density. They investigate the velocity of rise $\mathscr{V}$ of the intruding 'bubble' of less dense fluid and present a non-dimensional version of this velocity, which they call the Poiseuille number, Ps, as a function of $\gamma = \mu_U/\mu_L$, the ratio of the dynamic viscosities of the more dense fluid to the less dense fluid, where $Ps \equiv \mathscr{V}\nu_U/(g'R^2)$, ν_U is the kinematic viscosity of the upper, relatively dense fluid, g' is the reduced gravity and R the radius of the tube. They suggest no theory themselves, but compare their experimental results with the theoretical results of Kazahaya, Shinohara & Saito (1994), who derive a model for an inner, ascending Poiseuille flow surrounded by an outer, descending Poiseuille flow contained in a long cylinder of radius R. The experimental data do not fit the analysis of Kazahaya *et al.* (1994) at all well. Stevenson & Blake (1998) mention, in our opinion correctly, that (part of) the problem is the 'incorrect assumption of zero velocity at the interface between the two fluids' invoked by Kazahaya *et al.* (1994). They also describe three different overturn styles. For γ less than about 10, the descending fluid detaches from the wall and flows in the centre, surrounded by ascending fluid at the walls in the lower half of the tube. In mirror fashion, in the upper region the ascending fluid also detaches from the wall and rises through descending fluid around it. For $10 < \gamma < 300$ (approximately), the descending fluid splits into individual blobs that descend down the centre of the pipe. For $\gamma > 300$ the descending fluid sticks to the walls at all times with the ascending fluid rising in the center of the tube.

Stevenson & Blake (1998) were not able to measure accurately the radius of the ascending fluid region in their main experiments because of optical distortion. However, they considered four additional experiments in which low-viscosity fluid was injected into denser, more viscous fluid at the base of a vertical open-ended column. They found that the relative radius (the radius divided by the radius of the containing tube) for these ascending regions looked similar as in their main experiments and was approximately constant with values of 0.53–0.64 for four experiments with a reasonably broad ranges of Ps and γ.

Why is this the form of motion? They make no comment as to why the fluid tends to ascend in the central regions rather than in the outer regions. One might immediately think that the no-slip condition at the wall plays an important role here, but it is not obvious how to evaluate this quantitatively. They also make no comment on reasons for the cross-sectional area of the rising fluid.

The geological/geophysical motivation for this activity comes from measurements of fluxes of sulphur dioxide and other volatiles from lava lakes in volcanic craters. The investigations tend to concentrate on the sulphur dioxide fluxes because these are much easier to measure, by infrared remote sensing techniques, than the possibly much larger fluxes of water vapour or carbon dioxide. Evaluation of the amount of magma (liquid rock) required to come to the surface to supply the sulphur dioxide flux can be calculated from the known (low) amount of sulphur dioxide dissolved in and transported by the magma. This value of magma flux can exceed by as much as four orders of magnitude the actual erupted flux (Francis, Oppenheimer & Stevenson 1993; Wallace 2001). The proposed explanation for this discrepancy is that magma relatively rich in sulphur dioxide rises from a holding reservoir (magma chamber), which exist in the Earth's crust a few kilometres beneath volcanic craters. As the magma rises, the pressure decreases, which leads to degassing of the sulphur dioxide (and some crystallization; see Jaupart 2000 or Sparks 2003 for example). The degassed sulphur dioxide travels mainly at the same velocity as the rising magma because it is in the form of small bubbles, so the argument runs, but when the magma reaches the

surface the gas can escape. This leaves the magma with an increased density, which is further increased by the cooling that occurs, and also by crystallization. The relatively heavy magma then sinks down the conduit – making for a bi-directional flow within the conduit – and this 'conveyor-belt' form of motion can continue, transporting sulphur dioxide to the surface and then into the atmosphere, without a net flux or eruption of any magma. The rate of flow in the conduit is partly determined by the change in density, which is itself set by the heat transfer between the lava lake and the atmosphere. However, attractive as the whole explanation may be, no complete mathematical analysis to test the idea quantitatively has been conducted.

The aim of the current paper is to develop the quantitative analysis supported by laboratory experimentation and then to briefly apply the results to the geological problem. We investigate here the flow that results when relatively dense, viscous liquid flows from a sealed container down a vertical pipe into another container, initially filled with relatively less dense viscous liquid. This situation is first investigated experimentally and a quantitative explanation of the experimental data is then presented. We hope to publish a fuller discussion of the geological consequences of our results in a journal specializing in the Earth sciences.

The form of the paper is as follows. In the next section, by way of setting up a foundation, we consider the emptying of an open container through a simple hole in its base over a range of Reynolds numbers. By dimensional arguments we will construct the expected form of a non-dimensional flux versus Reynolds number at the limits of low and high Reynolds number and show experimentally how to link these two. In § 3, experiments for the interchange of dense fluid filling a closed upper container with relatively less dense fluid beneath it will be described, leading to the relationship between a non-dimensional transport number Te and γ. Section 4 will present the mathematical analysis of a simplified, steady and axisymmetric, fluid-mechanical model, incorporating the effects due to gravity and the unknown pressure gradient. The final section presents our conclusions and a brief description of the geological relevance of the work.

2. Flow from a hole in a container

In order to set the foundations, consider a container filled with liquid of density ρ and kinematic viscosity ν to a height h open to the atmosphere draining through a hole in the bottom with a scale (like the radius) of r. For large Reynolds numbers $Re = Vr/\nu$, where V denotes the exit velocity scale, it follows from Bernoulli's principle that $V \propto (gh)^{1/2}$, where g is the acceleration due to gravity. Thus the volume flux $Q \propto (gh)^{1/2}r^2$, with the constant of proportionality dependent on the details of the hole. In summary, the non-dimensional flux F given by

$$F \equiv Q/[r^2(gh)^{1/2}] \sim \text{constant} \qquad (R' \equiv (gh)^{1/2}r/\nu \gg 1), \tag{2.1}$$

with the value of the constant dependent on the coefficient of contraction or *vena contracta* (Batchelor 1967).

For small Reynolds number, balancing the driving pressure head ρgh with the viscous stress $\mu v/r$, where the dynamic viscosity $\mu = \rho\nu$, we determine that $V \sim ghr/\nu$, $Q \sim ghr^3/\nu$ and $Re \sim ghr^2/\nu^2$, with the constant of proportionality discussed in Happel & Brenner (1973). In summary

$$F \sim R' \qquad (R' \ll 1). \tag{2.2}$$

To test these hypotheses and scaling and to determine the relationships for moderate R', we carried out a series of simple laboratory experiments.

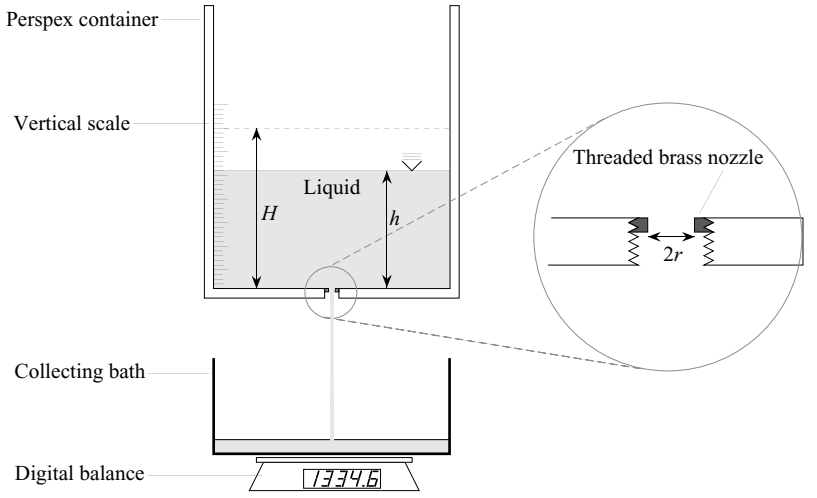

FIGURE 1. The experimental apparatus used for measuring the flow from a rectangular container.

#	Hole radius (cm)	Liquid	Density ($g\,cm^{-3}$)	Viscosity ($cm\,s^{-1}$)
1	0.50	Pure water	0.9982	0.01
2	0.35	Pure water	0.9982	0.01
3	0.35	100 wt % glycerine	1.2600	7.70
4	0.50	100 wt % glycerine	1.2600	7.70
5	0.50	70.3 wt % glycerine	1.1820	0.175
6	0.35	70.3 wt % glycerine	1.1820	0.175
7	0.35	80.0 wt % glycerine	1.2085	0.399
8	0.35	92.0 wt % glycerine	1.2404	1.83
9	0.50	92.0 wt % glycerine	1.2404	0.83

TABLE 1. A listing of the hole radius and liquid properties for the various drainage experiments. Density values were determined by hydrometer and viscosity values were measured by U-tube viscometers.

The experimental apparatus consisted of an open-topped Perspex box with a square base of internal length 25 cm and height 30 cm, as shown in figure 1. The fluid in the container drained through a circular hole of radius r drilled through the centre of a 3 mm thick brass disk of diameter 16 mm, which was screwed into a threaded hole in the centre of the base. Two interchangeable brass disks were used, with hole radii of 0.5 cm and 0.35 cm. The box was supported above a collecting bath sitting directly on an electronic balance which could measure mass in the range 0–6 kg to an accuracy of 0.1 g. At the start of each experiment, the outlet hole was temporarily stoppered and the Perspex container filled to a height H (approximately 7.5 cm). The stopper was then removed and the liquid allowed to drain freely into the collecting bath beneath. Throughout the drainage, the height h of the free surface of liquid remaining in the container and the mass of liquid M in the collecting bath were both recorded as functions of time until the container was empty.

A total of nine different combinations of hole radius and liquid viscosity were explored, as listed in table 1. Each experiment was conducted three times and averaged

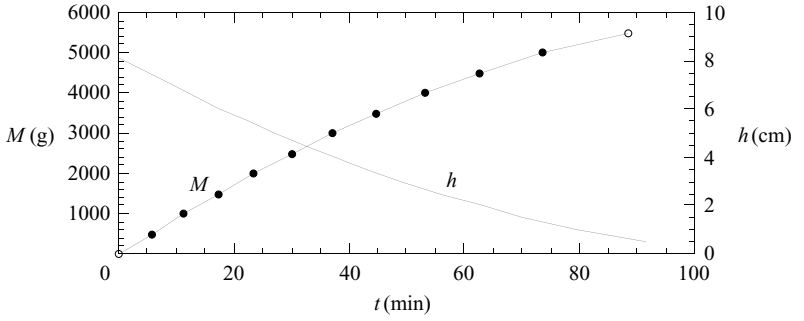

FIGURE 2. Mean measurements of the height h of liquid in the container and the mass M of liquid collected in the bath as functions of time t for a typical drainage experiment (#5 in table 1). Values of Q were calculated for given values of h for each point marked with a solid circle from the differences of data points on either side.

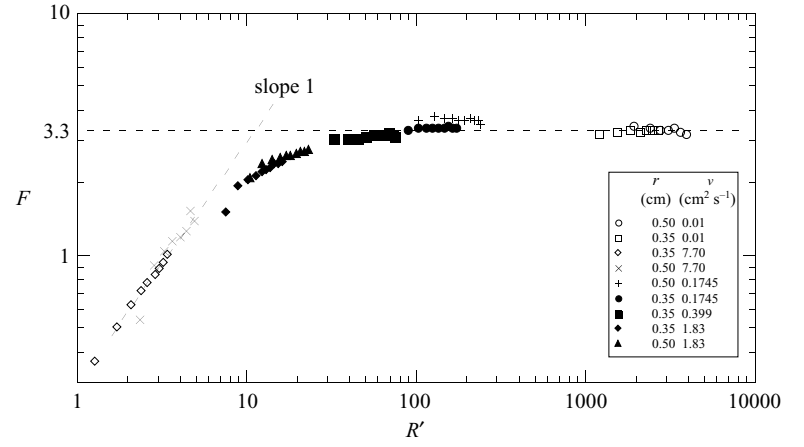

FIGURE 3. Plot of F as a function of R' for the drainage experiments. Each array of data comes from a single experiment, and tracks the decrease in Q with decreasing h.

values used in the subsequent analyses with differences of order 2%. The liquids used were water, glycerine and mixtures thereof, as specified in table 1 along with their relevant physical properties. In order to determine the relationship for the flux rate as a function of height and to test the theoretical relationships given by (2.1) and (2.2), it was necessary to calculate the volumetric flux Q. Since this flux decreased as the head of liquid in the container fell during the course of each experiment, a differencing method was adopted to evaluate the mean volumetric flow rate at several specific values of the hydrostatic head h as it reduced, as detailed in figure 2.

Figure 3 plots F as a function of R'. We see that (2.1) and (2.2) are appropriate except for $7 \lesssim R' \lesssim 30$, in which range the relationship between F and R flares smoothly between (2.1) and (2.2).

If the container is closed, much more interesting phenomena can occur, because compressibility effects become important. We have begun a preliminary series of experiments in which a sealed cylinder (of radius 7.9 cm and height 16.9 cm) filled with water drains through a long vertical tube (length ~ 100 cm, diameter ~ 1 cm) sealed into the centre of the base. Initially, a plug of air rises up the centre of the tube while water drains at a steady rate from its base. Once the plug of air reaches

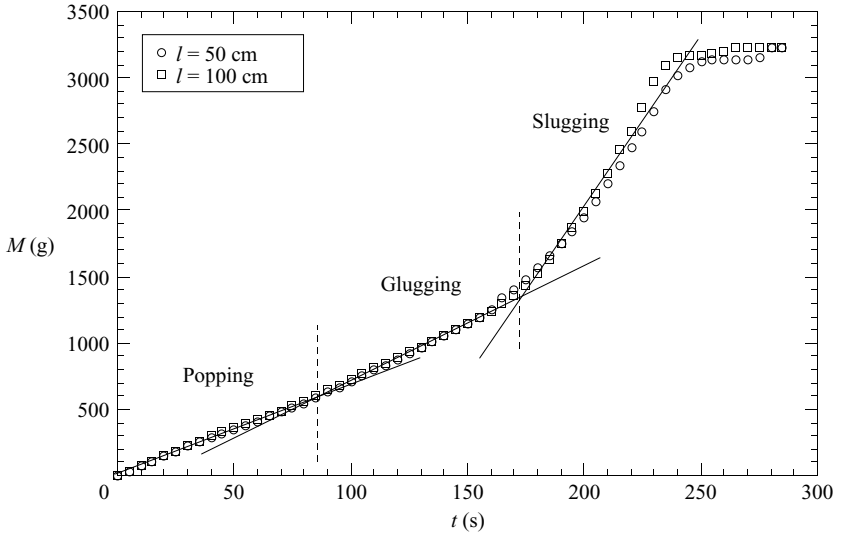

FIGURE 4. The mass of water collected below the exit tube as a function of time for two different long tubes. Straight-line fits to the three separate regimes are also included.

the base of the cylinder, bubbles of air are released into the cylinder at a regular frequency, and collect as a layer of air beneath the closed roof. From the acoustic signal emitted during this process we call this regime 'popping'. This air layer grows in thickness, until, after approximately 80 s, a second regime (which we call 'glugging') occurs, during which plugs of water are drawn down the tube to a length l, which creates a partial vacuum at the top of the cylinder. The difference in pressure draws the plug back up into the cylinder along with some air. This process is repeated with a frequency that steadily decreases while the maximum length of drawdown l steadily increases until it attains the full length of the drainage tube. At this stage, after about 180 s, a third regime (which we call 'slugging') is encountered. During this regime, a prolonged flow of water streams out of the tube until the partial vacuum created in the cylinder causes the whole column of water in the tube to be powerfully accelerated back into the chamber in fountains which became progressively more violent, until after about 230 s the cylinder is fully evacuated. Movie 1, available with the online version of the paper, presents short clips of each of these forms of motion.

We have measured the mass of the drained water as a function of time; this is depicted in figure 4 for tubes of length 50 and 100 cm. During the popping stage the mass discharge rate is approximately constant at $6.5\,\mathrm{g\,s^{-1}}$; during the glugging stage it is $8.9\,\mathrm{g\,s^{-1}}$; while during the slugging stage it is $26.5\,\mathrm{g\,s^{-1}}$. There are antecedents of this behaviour, but for the different situation of a relatively short tube, discussed by Clanet (2000) and Clanet & Searby (2004). The geometry of their apparatus (incorporating only a short delivery tube) does not yield the three regimes as shown in figure 4. We plan to present a full experimental and theoretical description of the phenomena in a future publication. Here we include a preliminary description mainly for comparison.

3. Bi-flow between two sealed containers

Motivated in part by the geological application, we conducted two series of experiments aimed at investigating the buoyancy-driven exchange of fluids between

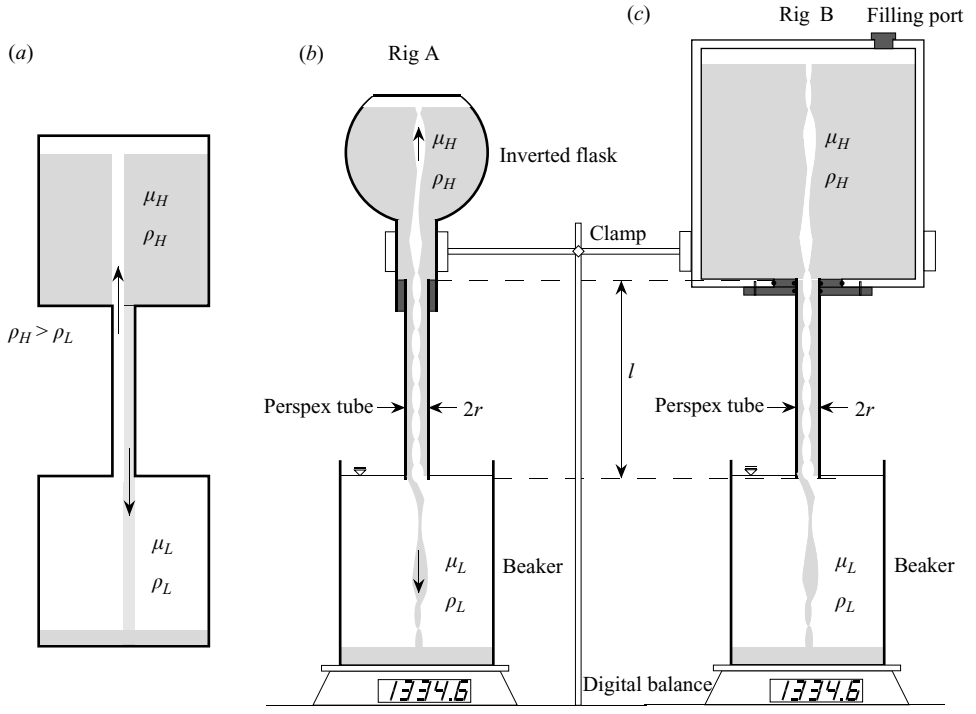

FIGURE 5. The apparatus used for the exchange flows. (*a*) Schematic of the system. (*b*) Preliminary set-up used for experiments A1–A33. (*c*) Improved set-up used for experiments B34–B56.

two reservoirs linked by a vertical conduit or tube. A schematic of the set-up is shown in figure 5(*a*). Relatively dense fluid contained in the closed, upper reservoir is connected by a thin vertical tube to a lower reservoir initially containing less dense fluid. The density difference between the two fluids results in a buoyancy-driven exchange flow, with a downward volumetric flux of the denser fluid being matched by an equal upward volumetric flux of the less dense fluid. This exchange continues until less dense fluid is no longer below more dense fluid.

We investigated the fluid interchange by measuring the exchange flux for different values of the tube radius, the tube length, the initial density difference between the two fluids and their relative viscosities. Since there is no net volume flux through the tube, in a closed system we could not initially think of a practical, non-intrusive way to measure the actual volumetric rate of exchange of each fluid. We solved this problem, however, by measuring the change in mass of the lower reservoir as a function of time. This was achieved using an open-topped lower reservoir, and submerging the tip of the connecting conduit just below the free surface of the contained liquid. The conduit itself was sealed at its upper end into the base of the upper reservoir, both of which were clamped to a rigid stand. The lower reservoir thus did not support weight from the conduit or upper reservoir, and by placing it on an electronic balance, the mass of the liquid in the lower reservoir could be measured with time as it increased throughout the exchange. The drawback of this measuring system is that the mass flux so obtained can only be related to the volumetric flux if the densities of the exchanging fluids are known and no mixing takes place between them within the conduit. With this limitation in mind, a number of experiments were performed with

immiscible fluids, thereby eliminating the problem induced by mixing of the fluids. For experiments in which the exchanging fluids were miscible and mixing did occur in the conduit, a separate analysis of the results is necessary and will be detailed later.

In practice, two experimental rigs were employed, as shown in figure 5. A series of preliminary experiments (denoted by the prefix A) was first conducted in the simple set-up depicted in figure 5(*b*), in which an inverted, 1 litre, round-bottomed flask served as the upper reservoir. Perspex tubes of different lengths and radii were fixed into the neck of the flask using silicone sealant and corks, and these projected vertically down such that their lower ends were submerged just beneath the free surface of the fluid in the lower reservoir. Thirty-three experiments (A1–A33) performed in this system produced satisfactory results, but the non-ideal entry conditions into the tube through the neck of the flask, its limited volume and the awkwardness of exchanging and re-sealing the various conduit tubes led eventually to the custom-built improved apparatus shown in figure 5(*c*). In this modified set-up, the upper reservoir was replaced by a Perspex container having a circular base of internal radius 7.9 cm and height 16.9 cm, and a working volume of 3.2 litres. The reservoir could be filled through an access port in the sealed lid, and was drained through a fixture in the centre of the base which allowed easy, O-ring sealed push-fit interchange between Perspex tubes of three different radii and any desired length. The 23 experiments performed in this set-up are denoted by the prefix B, as detailed in table 2 (available as a supplement to the online version of the paper) which gives the initial conditions and parameters for all the bi-flow experiments. While the geometrical set-up for series B was better than that for series A, the results obtained from each seemed equally reliable.

A variety of fluids were used to explore a wide range of different density and viscosity contrasts. The less dense fluids contained in the lower reservoir covered a viscosity range from 0.01 to 63 $\mathrm{cm^2\,s^{-1}}$, and included pure water, various aqueous glycerine solutions, vegetable oils and high-viscosity polymer solutions of carboxymethylcellulose (CMC). The more dense fluids initially contained in the upper reservoir ranged in viscosity from 0.01 to 450 $\mathrm{cm^2\,s^{-1}}$, and included pure water, various aqueous salt and glycerine solutions, and pure golden syrup. With the exception of water, the density and viscosity of each solution used were determined prior to each run using hydrometers and U-tube viscometers respectively. Each experiment began by filling the upper reservoir and conduit tube with a known mass of fluid m_U, initially held in place by a temporary stopper at the lower end of the tube. The lower reservoir was then filled with a mass m of dense solution until the lower tip of the conduit tube was just submerged below the free surface. The exchange began upon removal of the stopper, and the increasing mass of the lower reservoir was recorded as a function of time until the exchange ceased.

Several different styles of exchange flow were observed depending on the viscosities of the fluids involved and whether they were miscible with each other. The main styles of flow behaviour may be summarised by the schematic representation shown in figure 6 and movie sequences 2 to 5 (available with the online version of the paper). When both fluids were relatively inviscid and miscible (figure 6*a*), vigorous turbulent mixing of the fluids took place in the conduit, such that mixed fluid emerged from either end of the tube into the upper and lower reservoirs as plumes, which proceeded to occupy the reservoirs in a typical filling box fashion. Figure 6(*b*) depicts the situation where both fluids have relatively low viscosities but are immiscible. In this type of exchange, the upward-moving less dense fluid forms an almost straight-sided column rising up through the centre of the tube with an outer annulus of dense fluid moving in the opposite direction. The situation shown in figure 6(*c*) relates

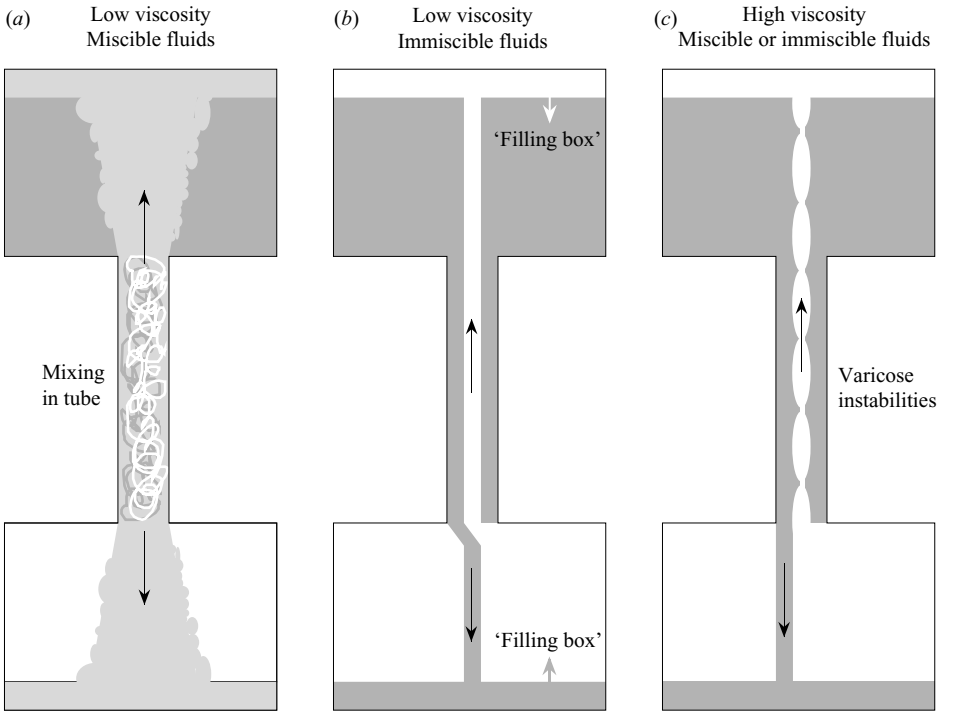

FIGURE 6. Sketches of three different styles of exchange. (*a*) When both upper and lower fluids are miscible with each other and have low viscosity, vigorous turbulent mixing occurs throughout the length of the tube. (*b*) When the fluids are immiscible but still have relatively low viscosity, the exchange occurs as a straight-sided column of the less dense fluid moving upwards through a surrounding envelope of downward-moving dense fluid. (*c*) When one or both of the fluids have high viscosity and are prevented from mixing, either due to this viscosity contrast or because they are immiscible, the exchange flow occurs as an irregular column of upward-moving fluid with varicose instabilities. This column may be confined to the central axis of the tube, with a surrounding annulus of dense, downward-moving fluid, or it may be highly irregular and break into discrete blobs or partially adhere to the sidewall of the conduit.

to the situation where one or both of the fluids have relatively high viscosity, and are prevented from mixing either due to their viscosity contrast or because they are physically immiscible. In this case, the exchange flow occurs as an irregular column of upward-moving fluid, which develops varicose instabilities. The upward flow may be confined to the central axis of the conduit, or it may be highly irregular and break into discrete blobs or partially adhere to the sidewalls of the conduit.

The only quantitative data that were measured from the experiments was the mass of the lower reservoir M as a function of time. The interpretation of these data differs according to whether any mixing of the two fluids occurred during the exchange, and is shown in figure 7. Schematic representations of M as a function of time are shown for cases where there is no mixing (figure 7*a*), and where mixing does occur (figure 7*b*).

With no mixing (figure 7*a*) there is a steady increase in M as the fluids exchange until one of the reservoirs is emptied of its initial fluid. In our experiments, the upper reservoir always had the smaller volume and was thus exhausted first. Assuming no mixing, from conservation of mass and volume we can calculate the theoretical final

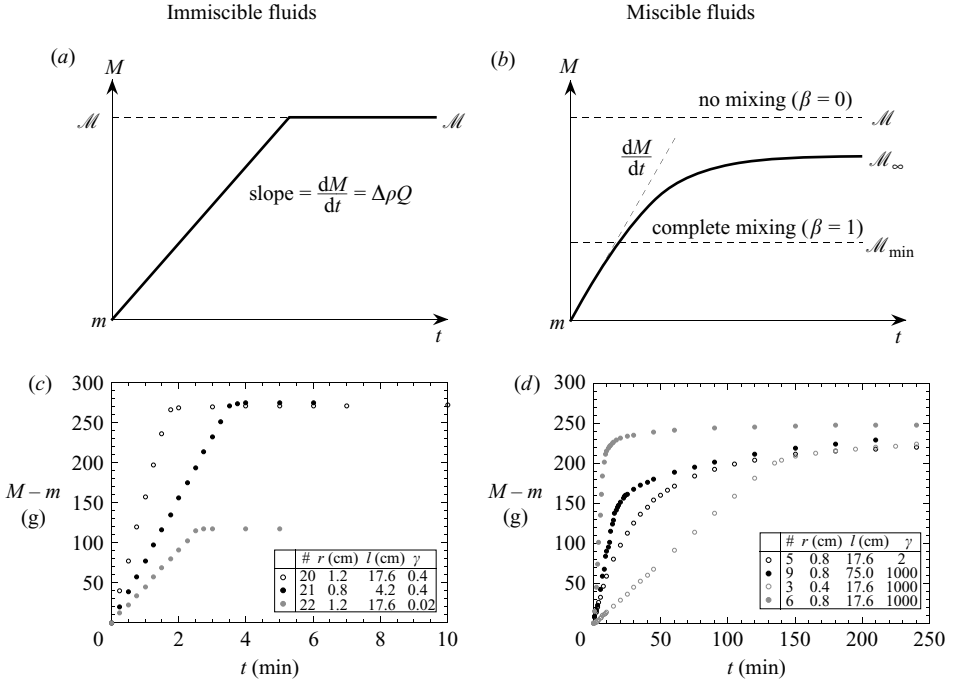

FIGURE 7. Schematic representations of the mass of the lower reservoir, M, with time for (a) immiscible and (b) miscible fluids. In (b) the final mass of the lower reservoir $\mathscr{M}_\infty$ lies between the two theoretical limits of no mixing $\mathscr{M}_{\min}$ and complete homogenization of all the fluid in the system ($\mathscr{M}$). A mixing ratio β, defined as $(\mathscr{M}-\mathscr{M}_\infty)/(\mathscr{M}-\mathscr{M}_{\min})$, can be used to quantify the degree of mixing. Representative experimental data of $M-m$ for immiscible and miscible fluids are shown in (c) and (d) respectively.

mass of the lower reservoir $\mathscr{M}$ as

$$\mathscr{M} = m + (m_U \Delta\rho/\rho_U), \tag{3.1}$$

where ρ_U and ρ_L are the densities of the fluid in the upper and lower reservoirs respectively, and $\Delta\rho = \rho_U - \rho_L > 0$. The mass of the lower reservoir increases linearly with time up to this theoretical maximum and then exchange ceases. The mass flux $\mathrm{d}M/\mathrm{d}t$ is then related to the volumetric flux Q by

$$Q = \frac{\mathrm{d}M}{\mathrm{d}t}/\Delta\rho. \tag{3.2}$$

Figure 7(c) shows some representative data for experiments using immiscible fluids for which there can be no mixing. In each case, the final measured and predicted value for the final mass of the lower reservoir are equal to within experimental error (2%).

In figure 7(b), we consider the situation where some degree of mixing between the two fluids can take place during the exchange. The rate of mass exchange is no longer constant, but decreases steadily, and the mass asymptotes to a final value $\mathscr{M}_\infty$, which falls short of the theoretical maximum $\mathscr{M}$. From the initial masses of fluids in both reservoirs, it is also possible to calculate a minimum value for the final mass in the lower reservoir $\mathscr{M}_{\min}$ based on complete homogenization of all the fluid in the closed

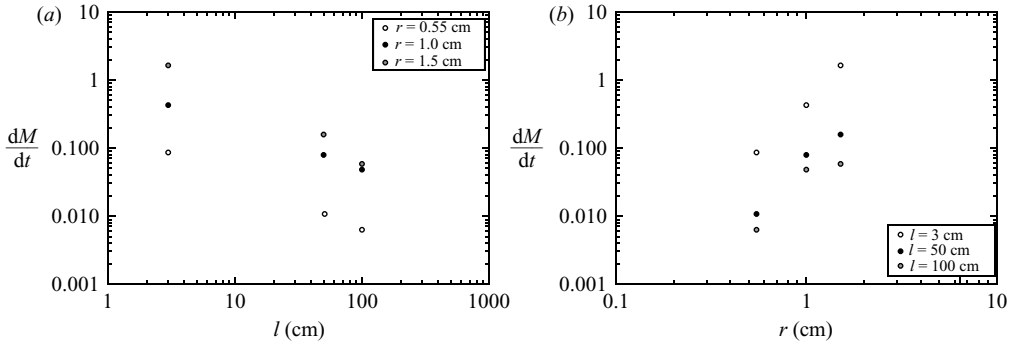

FIGURE 8. The initial rate of mass exchange measure as a function of (*a*) length of tube and (*b*) radius of tube.

system, which, again using conservation of mass and volume, is given by

$$\mathscr{M}_{\min} = m + \frac{m_U \Delta\rho/\rho_U}{1 + (\rho_L m_U/\rho_U m)}. \tag{3.3}$$

Using the theoretical maximum and minimum final values, we can use the experimentally measured final value of $\mathscr{M}_\infty$ to provide a quantitative estimate of the amount of mixing that must have occurred, expressed as a mixing fraction β, where

$$\beta = \frac{\mathscr{M} - \mathscr{M}_\infty}{\mathscr{M} - \mathscr{M}_{\min}}. \tag{3.4}$$

A value of $\beta = 0$ indicates no mixing at all, while $\beta = 1$ represents complete homogenization of the two fluids.

Figure 7(*d*) presents some representative experimental data in which some mixing occurred. In these experiments, the mass flux $\mathrm{d}M/\mathrm{d}t$ is defined by a fit to the data in the initial linear stage, and the volumetric flux Q is then derived from this using (3.2). Calculated values of Q and β for all experiments are presented in table 2.

Mixing of the exchanging fluids in the conduit has the important effect of reducing the rate of exchange, since it decreases the density difference driving the flow. We investigated the influence on mixing of the radius and length of the conduit by conducting a systematic series of experiments (B45–B53) using low-viscosity miscible fluids (water and 50 wt % glycerine) in apparatus B. A 3×3 matrix of experiments was run for tube radii of 0.55 cm, 1.0 cm and 1.5 cm and tube lengths of 3 cm, 50 cm and 100 cm. The rates of initial mass exchange as functions of tube radius r and tube length l, keeping all other parameters fixed, are shown in figure 8.

The flow regime is clearly too complicated to describe in detail by two steady uni-axial flows in opposite directions, although we will examine the consequences of this approach in the next section. Here we extend the arguments of the previous section to develop asymptotic results in the limits of large and small γ and large and small Reynolds numbers.

The flow takes place under a balance between the vertical driving force per unit cross-sectional area due to buoyancy, $\Delta\rho g R$, where R is the radius of the connecting tube; the vertical pressure difference, which is also of order $\Delta\rho g R$; the viscous stresses $\mu V/R$, where V is a scale for the velocity within the connecting pipe (the maximum upward velocity, for example) and μ is *a* viscosity (to be defined in detail below); and the inertial force ρV^2. For extremely viscous, low-Reynolds-number flow $\rho V R/\mu \ll 1$, buoyancy forces balance viscous forces to lead to $V \sim \rho g' R^2/\mu$, where $g' = \Delta\rho g/\rho$ is

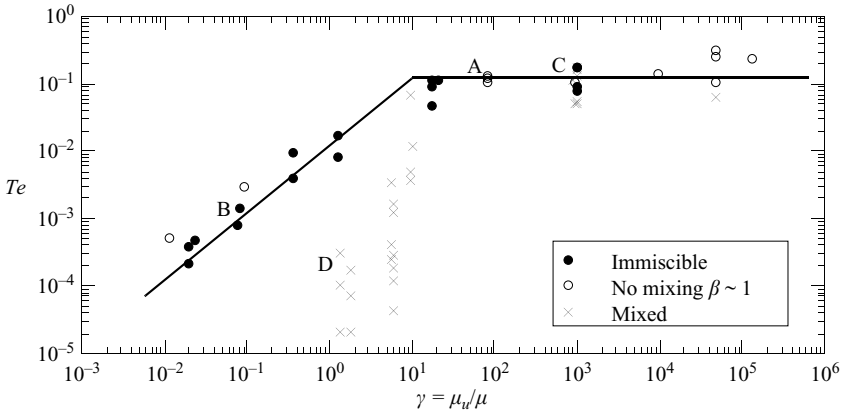

FIGURE 9. Plot of Te as a function of γ. The straight-line portions represent $Te = 0.01\gamma$ and $Te = 0.125$, valid for $\gamma \ll 1$ and $\gg 1$ respectively. The letters A, B, C and D indicate the flow parameters for movie sequences 2, 3, 4, 5 respectively.

the reduced gravity. Thus the volume flux in either fluid $Q \sim \rho g' R^4/\mu$. Alternatively, for high-Reynolds-number flows, $\rho V R/\mu \gg 1$, a balance between buoyancy and inertial forces indicates that $V \sim (g'R)^{1/2}$ and $Q \sim (g'R)^{1/2} R^2$.

A non-dimensional transport number Te can be defined by

$$Te = \mu_U Q/(g \Delta\rho R^4). \tag{3.5}$$

Thus, for low Reynolds numbers, $Te \sim \mu_U/\mu$. If $\mu_U \gg \mu_L$, most of the viscous dissipation is due to the upper fluid and μ should be identified as μ_U; and then Te is constant. If, on the other hand, $\mu_L \gg \mu_U$, μ should be identified as μ_L; and then $Te \sim \gamma$. These two limiting curves are plotted with all the experimental data in figure 9, where solid circles indicate data obtained from experiments with immiscible fluids; open circles from experiments with miscible fluids but little mixing, $\beta \sim 1$; and crosses from experiments in which considerable mixing took place. The two limiting lines provide a good fit to the data for experiments at low Reynolds numbers, while most of the data taken from experiments in which a considerable amount of mixing took place plot quite differently. Explicitly, the best fit curves to much of the experimental data are $Te = 0.01\gamma$ for $\gamma \ll 1$; and $Te = 0.125$ for $\gamma \gg 1$. The mismatch with some of the data suggests considering the limiting case for high Reynolds numbers, for which $Te \sim \nu_U/[(g'R)^{1/2} R] \equiv Re_U^{-1}$. Figure 10 presents Te as a function of Re_U. The data are seen to fit the limiting curves well, except for some experiments, for which the mixing was so strong that its effects need to be included in the force balance. In particular, the initial value of $\Delta\rho$ is not the appropriate density difference driving the fluids through the conduit. This change in conditions is seen to decrease the pre-multiplicative constant by about an order of magnitude, but not the functional form of Re_U^{-1}.

4. Theoretical discussion

A complete theoretical solution of the exchange flow, incorporating either or both of unsteady, non-axisymmetric flow in the conduit and mixing between the two fluids, is obviously impossible. Some initial understanding, however, can be gained from investigating the simplest, basic problem of assuming that the flow in the conduit is steady, coaxial and that no mixing takes place.

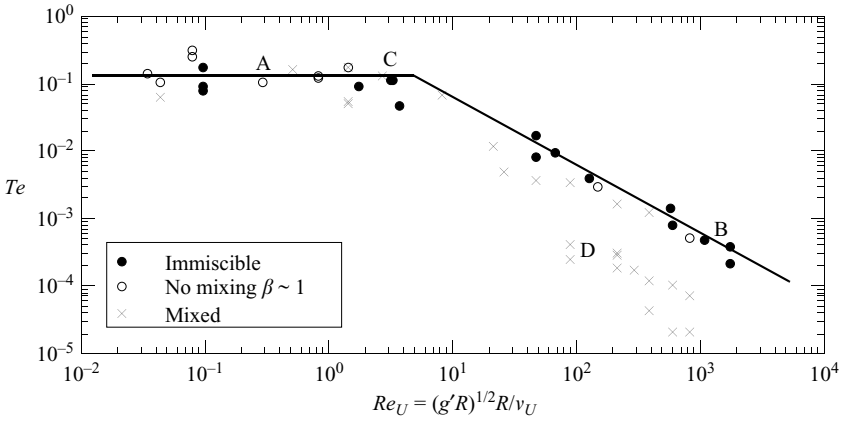

FIGURE 10. Plot of Te as a function of Re_U. The straight-line portions represent $Te = 0.125$ and $Te = 0.556 Re_U^{-1}$, valid for $Re_U \ll$ and $\gg 1$ respectively. The letters A, B, C and D indicate the flow parameters for movie sequences 2, 3, 4, 5 respectively.

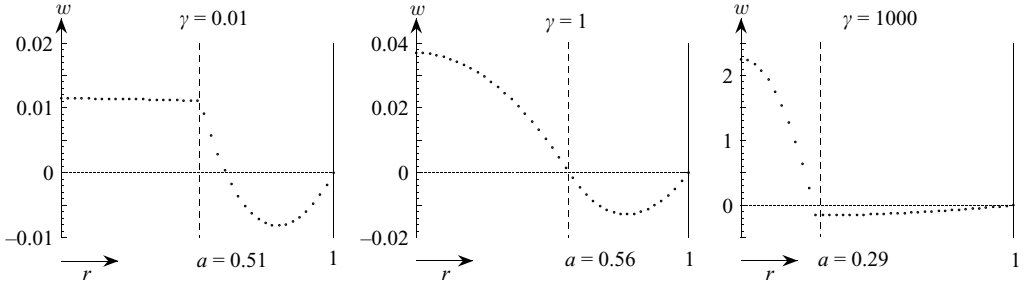

FIGURE 11. Typical velocity profiles as a function of radius, from (4.9), for $\gamma = 0.01$, 1 and 1000. The values of a and C used are those which maximise Te.

Linear stability analyses of such flows have been considered by a number of authors, including Hickox (1971), Joseph *et al.* (1997), and Scoffoni *et al.* (2001), who conclude, as discussed in the Introduction, that the flows are rarely if ever stable. How accurately a stable, axisymmetric flow will describe the mean fluid flux has not been previously determined, at least to our knowledge. That is our aim in this section.

Consider the steady-state flow depicted in figure 11, where there is an axial, inner flow in $0 \leqslant R \leqslant R_1$ and an outer flow in $R_1 \leqslant R \leqslant R_2$ acting under the force of gravity. The two regions move under a pressure gradient, p_z, and the difference in buoyancy between the two fluids. Assuming that the densities of the fluid are ρ_1 in the central region and ρ_2 in the outer region, we can write the governing equations as

$$0 = -\rho_1 g - p_z + \mu_1 \frac{1}{R}\frac{\mathrm{d}}{\mathrm{d}R}\left(R\frac{\mathrm{d}u}{\mathrm{d}R}\right) \qquad (0 \leqslant R \leqslant R_1), \tag{4.1a}$$

$$0 = -\rho_2 g - p_z + \mu_2 \frac{1}{R}\frac{\mathrm{d}}{\mathrm{d}R}\left(R\frac{\mathrm{d}u}{\mathrm{d}R}\right) \qquad (R_1 \leqslant R \leqslant R_2). \tag{4.1b}$$

The appropriate boundary conditions are

$$u(0) \quad \text{finite}, \qquad [u] = 0, \qquad \left[\mu\frac{\mathrm{d}u}{\mathrm{d}R}\right] = 0, \qquad u(R_2) = 0, \tag{4.2}$$

where

$$[\eta] \equiv \eta(R_1-) - \eta(R_1+). \tag{4.3}$$

One of the complications in this problem is that the pressure gradient p_z is initially unknown (as is R_1). We thus write

$$p_z = -\tfrac{1}{2}(\rho_1 + \rho_2)g - \tfrac{1}{2}g\Delta\rho C, \tag{4.4}$$

where C is to be determined later.

Introducing non-dimensional radii and velocities by

$$r = R/R_2 \quad w = \mu_2 u/\left(g\Delta\rho R_2^2\right), \tag{4.5}$$

the governing equations become

$$0 = \frac{1}{2}\gamma(C+1) + \frac{1}{r}\frac{\mathrm{d}}{\mathrm{d}r}\left(r\frac{\mathrm{d}w}{\mathrm{d}r}\right) \quad (0 \leqslant r \leqslant a), \tag{4.6a}$$

$$0 = \frac{1}{2}(C-1) + \frac{1}{r}\frac{\mathrm{d}}{\mathrm{d}r}\left(r\frac{\mathrm{d}w}{\mathrm{d}r}\right) \quad (a \leqslant r \leqslant 1), \tag{4.6b}$$

where

$$\gamma = \mu_2/\mu_1 \quad \text{and} \quad a = R_1/R_2, \tag{4.7}$$

which is yet to be determined. The appropriate boundary conditions are

$$w(0) \text{ finite} \qquad [w] = 0 \qquad \frac{\mathrm{d}w}{\mathrm{d}r}(a-) = \gamma\frac{\mathrm{d}w}{\mathrm{d}r}(a+) \qquad w(1) = 0. \tag{4.8}$$

The solutions to (4.6) and (4.8) are

$$w(r) = \tfrac{1}{8}\gamma(C+1)(a^2 - r^2) + \tfrac{1}{8}(C-1)(1-a^2) - \tfrac{1}{2}a^2\ln a \quad (0 \leqslant r \leqslant a) \tag{4.9a}$$

$$= \tfrac{1}{8}(C-1)(1-r^2) - \tfrac{1}{2}a^2\ln r \qquad (a \leqslant r \leqslant 1). \tag{4.9b}$$

The non-dimensional volume flux, q_1, in the central region is given by

$$(2\pi)^{-1}q_1 \equiv \int_0^a r w \mathrm{d}r \tag{4.10a}$$

$$= \tfrac{1}{32}\gamma(C+1)a^4 + \tfrac{1}{16}(C-1)a^2(1-a^2) - \tfrac{1}{4}a^4\ln a, \tag{4.10b}$$

while the non-dimensional volume flux, q_2, in the outer region is given by

$$(2\pi)^{-1}q_2 \equiv \int_a^1 r w \mathrm{d}r \tag{4.11a}$$

$$= \tfrac{1}{32}(C-1)(1-a^2)^2 + \tfrac{1}{8}a^2(1 - a^2 + 2a^2\ln a). \tag{4.11b}$$

The net vertical flux through any horizontal cross-section must be zero, and hence

$$q_1 + q_2 = 0, \tag{4.12}$$

which on adding (4.10b) and (4.11b) becomes

$$C[1 + (\gamma - 1)a^4] = (1-a^2)(1-3a^2) - \gamma a^4. \tag{4.13}$$

Figure 12 plots C as a function of a for various values of γ. It is immediately seen that for all a and γ, $-1 < C < 1$ and thus because C cannot be large or, in general, small, the effect of the pressure gradient involved in driving the flow is comparable to the additional body force difference. In particular in the limit $C = 1$, the vertical pressure gradient is just sufficient to balance the gravitational effects of the outer (falling)

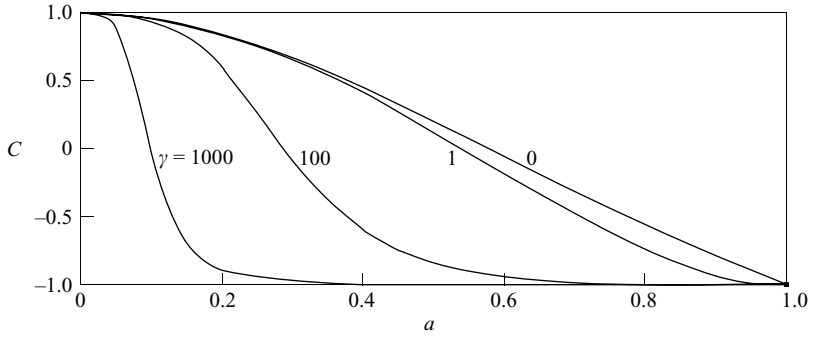

FIGURE 12. C as a function of a for four values of γ.

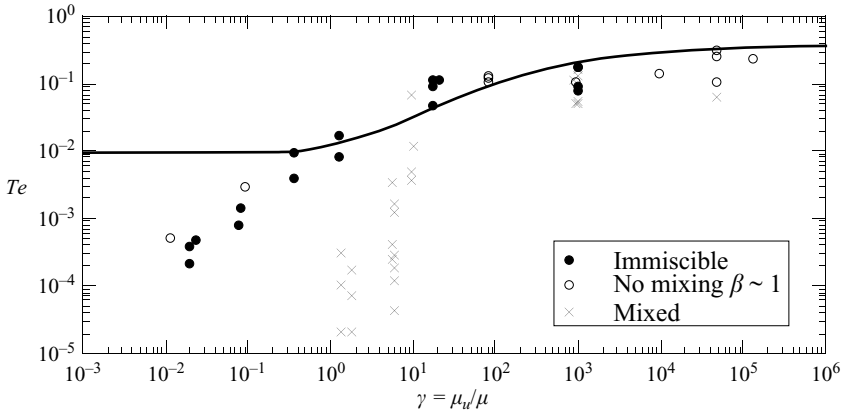

FIGURE 13. A plot of all the data. The solid curve represents the maximum flux (or Te) or maximum dissipation, D, according to a steady, axisymmetric analysis.

fluid, as seen in (4.6*b*). In contrast, in the limit $C = -1$, the vertical pressure gradient is just sufficient to balance the gravitational effects of the inner (rising) fluid, (4.6*a*). Also, for $\gamma < 1$, $C(a)$ is very insensitive to the value of γ and given approximately by $(1 - a^2)(1 - 3a^2)$, while for $\gamma > 1$, $C(a)$ is most sensitive to the value of γ.

The transport number

$$Te \equiv \frac{\mu_2 Q_1}{g \Delta\rho R_2^4} = q_1 = -q_2. \tag{4.14}$$

For given γ, either C or a still need to be determined by some extra criterion. This may be set by the details of the connection between the conduit and the containers, determining the ease with which the flow enters and exits the conduit and hence the local energy losses. An interesting exercise from a different perspective is to use the criterion that q_1, and hence Te, be a maximum. (The minimum is $Te = 0$, attained for $a = 0$ or 1 and $C = 1$ and -1 respectively.) Only by flowing in a non-axisymmetric or non-coaxial way could an experimentally determined Te exceed this value. Figure 13 plots this maximum value, $Te_{\max}$, as a function of γ. It is seen that the data generally lie just below the curve for $\gamma > 1$, and hence it is a good predictor, and definitely below it for $\gamma < 1$ and well below it for $\gamma \ll 1$. A steady, axisymmetric flow hence appears to yield reasonable predictions for the mean flux of fluid for $\gamma > 1$.

Another possible criterion is to extremize the dissipation Batchelor (1967), given by

$$\Phi = 4\pi \int_0^{R_2} \mu e_{ij} e_{ij} R \mathrm{d}R, \tag{4.15}$$

where $e_{ij} = (1/2)\mathrm{d}u/\mathrm{d}R$ is the strain rate tensor. Differentiating (4.9), inserting the results into (4.15) and carrying out the integrals, we evaluate the non-dimensional dissipation

$$D \equiv \int_0^a r \left(\frac{\mathrm{d}w}{\mathrm{d}r}\right)^2 \mathrm{d}r + \gamma \int_a^1 r \left(\frac{\mathrm{d}w}{\mathrm{d}r}\right)^2 \mathrm{d}r \tag{4.16a}$$

$$= \tfrac{1}{64}\gamma^2 (C+1)^2 a^4 + \gamma \left[\tfrac{1}{64}(C-1)^2(1-a^4) + \tfrac{1}{8}(C-1)a^2(1-a^2) - \tfrac{1}{4}a^4 \ln a\right]. \tag{4.16b}$$

D is zero for $a = 0$ or 1 and has a maximum for $0 < a < 1$. The corresponding value of Te is identical to that obtained by maximising the flux. This is because in this steady-state flow the dissipation must equal the rate of release of potential energy, which is directly proportional to the flux of fluid.

5. Conclusions and geological applications

We have presented some new experiments on the exchange flow between a dense, viscous liquid initially in a closed container about a relatively less dense, viscous liquid linked by a vertical connecting tube. The flow in the tube and the two containers showed a variety of features dependent on the viscosity ratios of the two liquids and whether they were miscible with each other or not. The flow of miscible liquids at high Reynolds numbers, based on the density difference and tube radius, between about 10 and 10^4 involved vigorous mixing in the tube, with the mixed liquids emerging into the reservoirs as plumes which then penetrated the container in the well-known filling box manner. This mixing, which reduces the density difference driving the exchange flow, also reduces the flux and transport number Te. The use of immiscible or very viscous liquids lead to a more ordered, but still irregular, flow which could at times break down into discrete blobs.

Using dimensional analysis, we showed that the data could be well collapsed, for low Reynolds numbers, to

$$Te = 0.01\gamma \quad (\gamma \ll 1) \tag{5.1a}$$

and

$$Te = 0.125 \quad (\gamma \gg 1), \tag{5.1b}$$

in terms of the transport parameter Te, defined by (3.5) and the ratio of the dynamic viscosities γ. For high Reynolds numbers the experimental data were well represented by

$$Te = 0.556 Re_U^{-1} \quad (Re_U \gg 1). \tag{5.2}$$

A simple theoretical model, incorporating a steady, axisymmetric core-annular flow yielded good agreement with the experimental data for $\gamma \gg 1$, with less agreement for flows with either $\gamma \ll 1$ or large values of Re_U.

Additional features would no doubt arise if the connecting tube was at an angle or if it was a slot with considerably different length scales in the two horizontal directions; and we plan to investigate these geometries in the near future.

There are many examples of volcanic craters with large sulphur dioxide (SO_2) fluxes. The largest of these include: Mt Etna in Italy, from which the typical flux is $50\,\mathrm{kg\,s^{-1}}$ or 5000 t/day; Mt Masaya in Nicaragua (1000 t/day); Mt Langila in Papua New Guinea (1000 t/day); Mt Erebus in Antarctica (300 t/day) (Francis *et al.* 1993); and Erta 'Ale in Ethiopia (100 t/day) (Oppenheimer *et al.* 2004).

The composition and viscosities of the magmas which feed these craters are all different. So also is the ratio $\mathscr{S}$ of the measured flux of SO_2 compared with that estimated from merely the erupted volume of magma. For Mt Etna $\mathscr{S} \sim 50$; for Mt Masaya $\mathscr{S} \sim 2,500$; and for Erta 'Ale $\mathscr{S}$ is effectively infinite, or it can maybe even be considered as negative because there has been a slow reduction in the height of the lava lake in the approximately thirty years of observations.

Typical viscosities might vary between $\mu_U \sim 2500\,\mathrm{Pa\,s}$, $\mu \sim 1500\,\mathrm{Pa\,s}$ ($\gamma = 5/3$) and $\mu_U \sim 10^5\,\mathrm{Pa\,s}$, $\mu \sim 10^4\,\mathrm{Pa\,s}$ ($\gamma = 10$). A typical $\Delta\rho$ is $70\,\mathrm{kg\,m^{-3}}$. The radius of the conduit (which may be neither uniform with depth nor vertical) could vary between 1 m and 10 m. Thus the volume flow rate in the conduit

$$Q = g\Delta\rho TeR^4/\mu_U\ \mathrm{m^3\,s^{-1}} \tag{5.3a}$$

$$\sim 100R^4/\mu_U\ \mathrm{m^3\,s^{-1}}, \tag{5.3b}$$

and could therefore take on values between 10^{-3} and $4 \times 10^2\,\mathrm{m^3\,s^{-1}}$. For a magma density of $2500\,\mathrm{kg\,m^{-3}}$ this means a mass flux between 2.5 and $10^6\,\mathrm{kg\,s^{-1}}$. Assuming 1 wt. % of the magma is made up of SO_2 (Wallace 2001), we calculate a SO_2 flux of between 0.025 and $10^4\,\mathrm{kg\,s^{-1}}$, which spans the observations.

Alternatively, because Q is such a strong function of R (5.3) we might argue the measured SO_2 flux could lead to indications of the conduit radius, which is difficult, if not impossible, to measure *in situ*. At Mt Etna, the observed SO_2 flux indicates that $Q \sim 50 \times 100/2500 = 2\,\mathrm{m^3\,s^{-1}}$. Hence, with $\mu_U = 2000\,\mathrm{Pa\,s}$ for the relatively inviscid basaltic Etna lava, $R \sim (40)^{1/4} \sim 2.5\,\mathrm{m}$, a reasonable estimate. A detailed comparison between the theory and field observations for specific sites will be presented in another publication.

We are grateful for John Hinch's continued interest and stimulating comments and the geological motivation provided by Steve Sparks and Clive Oppenheimer. In addition, all three provided insightful comments on an earlier version of the manuscript. The research of H. E. H. is supported by a Royal Society Wolfson Merit Research Award.

REFERENCES

Batchelor, G. K. 1967 *An Introduction to Fluid Dynamics*. Cambridge University Press.

Clanet, C. 2000 From Galilei to Torricelli. *Phys. Fluids* **12**, 2743–2751.

Clanet, C. & Searby, G. 2004 On the glug-glug of ideal bottles. *J. Fluid Mech.* **510**, 145–168.

Francis, P., Oppenheimer, C. & Stevenson, D. 1993 Endogenous growth of persistently active volcanoes. *Nature* **366**, 554–557.

Happel, J. & Brenner, H. 1973 *Low Reynolds Number Hydrodynamics*. Noordhoff.

Hickox, C. E. 1971 Instability due to viscosity and density stratification in axisymmetric pipe flow. *Phys. Fluids* **14**, 251–262.

Jaupart, C. 2000 Magma ascent at shallow levels. In *Encylopedia of Volcanoes* (ed. H. Sigurdson). Academic.

Joseph, D. D., Bai, R., Chen, K. P. & Renardy, Y. Y. 1997 Core-annular flows. *Annu. Fluid Mech.* **29**, 65–90.

Kazahaya, K., Shinohara, H. & Saito, G. 1994 Excessive degassing of Izu–Oshima volcano: Magma convection in a conduit. *Bull. Volc.* **56**, 2078–216.

Oppenheimer, C., McGonigie, A. J. S., Allard, P., Wooster, M. J. & Tsanev, V. 2004 Sulphur, heat, and magma budget of Erta 'Ale lava lake, Ethiopia. *Geol. Soc. Am.* **32**, 509–512.

Scoffoni, J., Lajeunesse, E. & Homsy, G. M. 2001 Interface instabilities during displacements of two miscible fluids in a vertical pipe. *Phys. Fluids* **13**, 553–556.

Sparks, R. S. J. 2003 Dynamics of magma degassing. In *Volcanic Degassing* (ed. C. Oppenheimer, D. M. Pyle & J. Barclay). Geol. Soc. London Spec. Pub. **213**, pp. 5–22.

Stevenson, D. S. & Blake, S. 1998 Modelling the dynamics and thermodynamics of volcanic degassing. *Bull. Volc.* **60**, 307–317.

Wallace, P. J. 2001 Volcanic SO_2 emissions and the abundance and distribution of exsolved gas in magma bodies. *J. Volcanol. Geotherm. Res.* **108**, 85–106.